Extreme heterochiasmy and high rates of sex-reversed recombination result in large yet homomorphic sex chromosomes in the Emei moustache toad

Siyu Xie, Jun Li, Wanyan Chen, et al.

Genome Res. 2025 35: 1325-1336 originally published online April 24, 2025
Access the most recent version at doi:10.1101/gr.280161.124

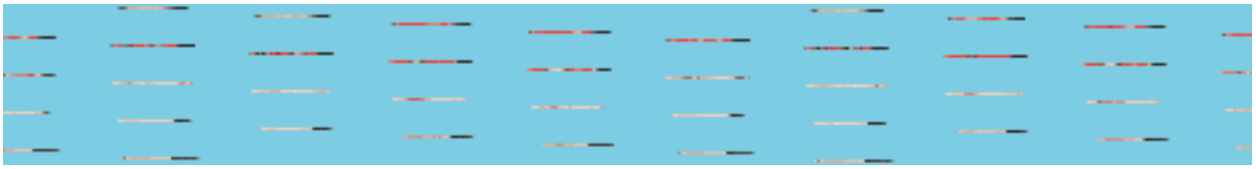

Research

Extreme heterochiasmy and high rates of sex-reversed recombination result in large yet homomorphic sex chromosomes in the Emei moustache toad

Siyu Xie,[1] Jun Li,[1] Wanyan Chen,[1] Lydia J.M. Fong,[2] Chunhua Huang,[1] Yan Feng,[1] Qingbo Ai,[1] Mian Zhao,[1] Judith E. Mank,[2] and Hua Wu[1]

[1]*Hubei Key Laboratory of Genetic Regulation and Integrative Biology, School of Life Sciences, Central China Normal University, Wuhan, Hubei, China 430079;* [2]*Department of Zoology and Biodiversity Research Centre, University of British Columbia, Vancouver, British Columbia V6T 1Z4, Canada*

Unlike the highly degenerated sex chromosomes in birds and mammals, many amphibians possess homomorphic sex chromosomes, which may result from high rates of sex chromosome turnover and/or occasional recombination between the X and Y (or Z and W) Chromosomes. Yet, the molecular basis for maintaining homomorphy remains elusive, particularly the power of rare recombination events to arrest sex chromosome divergence. Here, we identified sex chromosomes of the Emei moustache toad and examined potential mechanisms of maintaining homomorphy. Although the sex chromosomes are homomorphic, we observed an extensive region of X–Y genetic differentiation, spanning ~349 Mb, among the largest known to date in vertebrates. Despite this large size and the assumption that inversions catalyze recombination suppression between the X and Y Chromosomes, we found little evidence of XY structural variation. Using a high-density linkage map, we revealed that the large region of X–Y divergence was likely owing to the emergence of sex determining factors in the region of ancestrally low male recombination. Population genetic data showed high rates of sex-reversed XY-type females, and recombination between the X and Y Chromosomes in these individuals helps maintain the integrity of sequence and gene expression on the Y Chromosome. Finally, we revealed modest sexualization of gene expression within the sex chromosomes, and identified candidate genes involved in gonadal development. Our results not only show remarkable maintenance of vast sex differentiated regions under ancestral low recombination but also emphasize the sustaining power of X–Y recombination for homomorphic chromosomes over large genomic regions.

[Supplemental material is available for this article.]

The evolution of sex chromosomes represents one of the major innovations of inheritance and plays a core role in sexual evolution in the animal kingdom (Charlesworth 1991; Wright et al. 2016). In species with genetic sex determination mechanisms, sex chromosomes carry sex determination loci (Ellegren 2011) and diverge from one another once recombination between them is halted (Bull 1983; Charlesworth 1991; Wright et al. 2016; Carpentier et al. 2019). As a consequence of recombination suppression, deleterious mutations accumulate on the nonrecombining Y- or W-linked regions, which can eventually lead to degeneration and morphologically heteromorphic sex chromosome pairs (Charlesworth and Charlesworth 2000). For instance, the *Drosophila* neo-Y (Bachtrog et al. 2008) and human Y Chromosome (Livernois et al. 2012) have independently degenerated in part because of the accumulation of a large number of frameshift and nonsense mutations. Such heteromorphic sex chromosomes are widely found in therian mammals (Bellott et al. 2014; Cortez et al. 2014), neognath birds (Zhou et al. 2014; Bellott et al. 2017), snakes (Matsubara et al. 2006; Vicoso et al. 2013), and lepidopterans (Dai et al. 2024), among others.

In contrast to the stable and heteromorphic sex chromosomes in many clades, homomorphic sex chromosomes predominate in some vertebrate groups, with ~96% of amphibians and 90% of fishes exhibiting sex chromosomes that do not differ noticeably in size and shape (Eggert 2004; Bachtrog et al. 2014; Lambert et al. 2016). Current evidence suggests that all amphibians exhibit genetic sex determination (Bachtrog et al. 2014; Jeffries et al. 2018). However, sex chromosomes in the clade often exhibit limited regions that are characterized by suppressed recombination and low divergence levels between the X and Y, despite considerable age in some cases (Stöck et al. 2011). Why homomorphic sex chromosomes are so prevalent in amphibians and how long-term homomorphy is maintained are long-standing puzzles in sex chromosome evolution. Some have suggested that high rates of turnover can maintain homomorphic and young sex chromosomes in amphibians (Evans et al. 2012; Miura 2017; Jeffries et al. 2018). Another hypothesis posits that X–Y recombination occurs in sex-reversed individuals (XY females), halting X–Y divergence (Perrin 2009; Brelsford et al. 2016a). These alternatives have important implications for the maintenance and age of homomorphic sex chromosomes.

Homomorphic sex chromosomes are more challenging to study than heteromorphic sex chromosomes because of the low level of divergence between the X and Y. In amphibians, this is

Corresponding author: wuhua@ccnu.edu.cn
Article published online before print. Article, supplemental material, and publication date are at https://www.genome.org/cgi/doi/10.1101/gr.280161.124.

compounded by the scarcity of high-density genetic maps and large genome sizes. In recent years, research on the sex chromosomes of amphibians has employed methods such as microsatellite markers (Matsuba and Merilä 2009; Alho et al. 2010) and reduced-representation genome sequencing (Stöck et al. 2011; Brelsford et al. 2016b). However, these approaches yield a low density of markers, which hinders a detailed understanding of the causes and consequences of homomorphy on the gene content of sex-limited chromosomes (Brelsford et al. 2016c). Relying on whole-genome sequencing to compare genomic information between males and females not only allows for the accurate identification of sex chromosomes and provides higher resolution of the sex chromosomes but also enables the precise localization of sex-specific regions.

The Emei moustache toad (*Leptobrachium boringii*) is a species of the Megophryidae family and belongs to the early-diverged Archaeobatrachia suborder (Feng et al. 2017). It provides a good opportunity for examining mechanisms underlying homomorphic sex chromosomes in amphibians. Karyotype analysis has revealed that this species retains 13 chromosomes (Li and Fei 1990), which is close to the ancestral state of Anura (Bredeson et al. 2024). Additionally, *L. boringii* has rare male-biased sexual size dimorphism (present in just 7.5% of anurans), and breeding males usually develop keratinized nuptial spines on their upper jaws, a sexual ornament consistent with sexual selection (Zheng et al. 2008; Hudson and Fu 2013; Pincheira-Donoso et al. 2021). This enables the investigation of potential sexualization of sex chromosomes and its correlation with sexual dimorphism in moustache toads.

We generated a high-quality chromosome-scale genome assembly as a reference genome, in conjunction with phased haplotype genomes and transcriptomic data from both sexes. We identified the sex chromosomes and sex-linked region (SLR) of *L. boringii* and focused on the factors maintaining X–Y homomorphy. Using transcriptomic data across multiple tissues and developmental stages, we examined whether SLR gene expression is sexualized and identified candidate genes involved in sex determination and gonadal development. Based on comprehensive sequencing data, our main aim was to determine the status and potential mechanisms of maintaining homomorphic sex chromosome in *L. boringii*.

Results

Genome assembly and sex chromosome identification

We used a combination of long-read Pacific Biosciences (PacBio), short-read Illumina, and Hi-C data to produce the high-quality reference genome of a male *L. boringii*. Reads were first assembled into a conventional unphased reference genome (named as Lbor.v1) (Fig. 1A), which resulted in 3.38 Gb, with a contig N50 of 6.38 Mb and scaffold N50 of 406.89 Mb. A total of 99.8% of the sequences were assigned to 13 chromosomes. By using de novo prediction, homology searches, and transcript-based assembly, we identified 20,327 protein-coding genes in the *L. boringii* genome, of which 93.8% genes were functionally annotated. Genome completeness, as estimated by Benchmarking Universal Single-Copy Orthologs (BUSCO) (Simão et al. 2015) metazoa_odb9 as a reference, was demonstrated by the high percentage of complete BUSCOs of both the assembly (92.4%) and annotation (95.4%) (Fig. 1A; Supplemental Figs. S1, S2; Supplemental Tables S1–S9).

We used whole-genome resequencing to identify the SLR. The genomes of 20 individuals per sex of *L. boringii* were sequenced (average: 15× coverage) (Supplemental Data Set S1). We applied the Genome-Wide Association Study (GWAS) and male-to-female F_{ST} scans to our resequencing data. The results suggest that Chromosome 1 (Chr 1) is the sex chromosome pair (Fig. 1A), with significant association with sex and F_{ST} between sexes compared with other chromosomes (average F_{ST}-value of Chr 1: 0.122, other chromosomes: 0.002; $P < 2.22 \times 10^{-16}$, Wilcoxon rank-sum test).

To define the boundary of the pseudoautosomal region (PAR) and the SLR of *L. boringii*, we identified those regions with significant GWAS and F_{ST}-values. We identified highly concentrated and concordant *P*-values between GWAS and F_{ST} approaches in the SLR of Chr 1, whereas other regions in Chr 1 were identified as the PARs (for statistical thresholds, see Methods) (Fig. 1B; Supplemental Fig. S3). The SLR is ∼350 Mb in total length, spanning 101.14–450.89 Mb of Chr 1, occupying 60.78% of the chromosome and >10% of the entire genome. The two PARs are ∼101.14 Mb and ∼124.54 Mb in length, respectively. Compared with the SLR (average F_{ST}: 0.168), the PARs had lower differentiation (average F_{ST} of two PARs: 0.026 and 0.045).

We mapped whole-genome resequencing data of 20 individuals per sex against the reference genome (Lbor.v1) and identified 274,642 sex-specific SNPs based on the sex differences in allele frequencies (Brelsford et al. 2017). Of those, 274,384 (99.91%) SNPs were heterozygous in males and homozygous in females (Fig. 1B). Furthermore, 98.00% of these SNPs were located within the SLR of Chr 1 (Fig. 1B). This finding is consistent with the XY-type sex chromosome system. Despite the large size of the SLR, karyotype analysis indicated that Chr 1 of *L. boringii* is morphologically homomorphic in both female and male individuals (Fig. 1C,D; Supplemental Tables S10–S12). Therefore, we concluded that the *L. boringii* exhibits homomorphic sex chromosomes. Furthermore, Chr 1 in *L. boringii* has a high collinearity with Chr 1 of two other anuran species from different genera (*Xenopus* and *Bufo*), suggesting this chromosome pair is homologous across amphibians (Supplemental Fig. S4).

Low divergence and high collinearity between the X and Y Chromosomes

We phased PacBio HiFi data into two high-quality haploid genomes: HapA and HapB. All haploid genomes were separately assembled into 13 pseudochromosomes. The HapA genome assembly had a total length of 3.92 Gb, with a contig N50 of 25.34 Mb and a scaffold N50 of 437.49 Mb. The HapB genome was 3.74 Gb, with a contig N50 of 28.09 Mb and a scaffold N50 of 428.94 Mb. The complete BUSCO (Simão et al. 2015) of HapA and HapB was 95.25% and 94.67%, respectively, indicating high-quality genome assemblies for the *L. boringii* haplotypes (Supplemental Fig. S5; Supplemental Tables S13–S16).

To further identify the Y Chromosome, we used *k*-mer analysis to detect male-specific *k*-mers, often referred as Y-mers (Torres et al. 2018; Almeida et al. 2021; Kabir et al. 2022), from paired-end short reads of 20 males and 20 females (Supplemental Data Set S1). In an XY system, the number of female-specific *k*-mers (female-mers) represents the false-positive rate as *k*-mer analysis can have a high type-I error rate (Almeida et al. 2021). Consistent with the XY sex-determination system in *L. boringii*, we found more than 400-fold more Y-mers (79,341) than female-mers (177) (Supplemental Fig. S6). We further used Y-mers and female-mers to identify the Y haplotype from the HapA and HapB

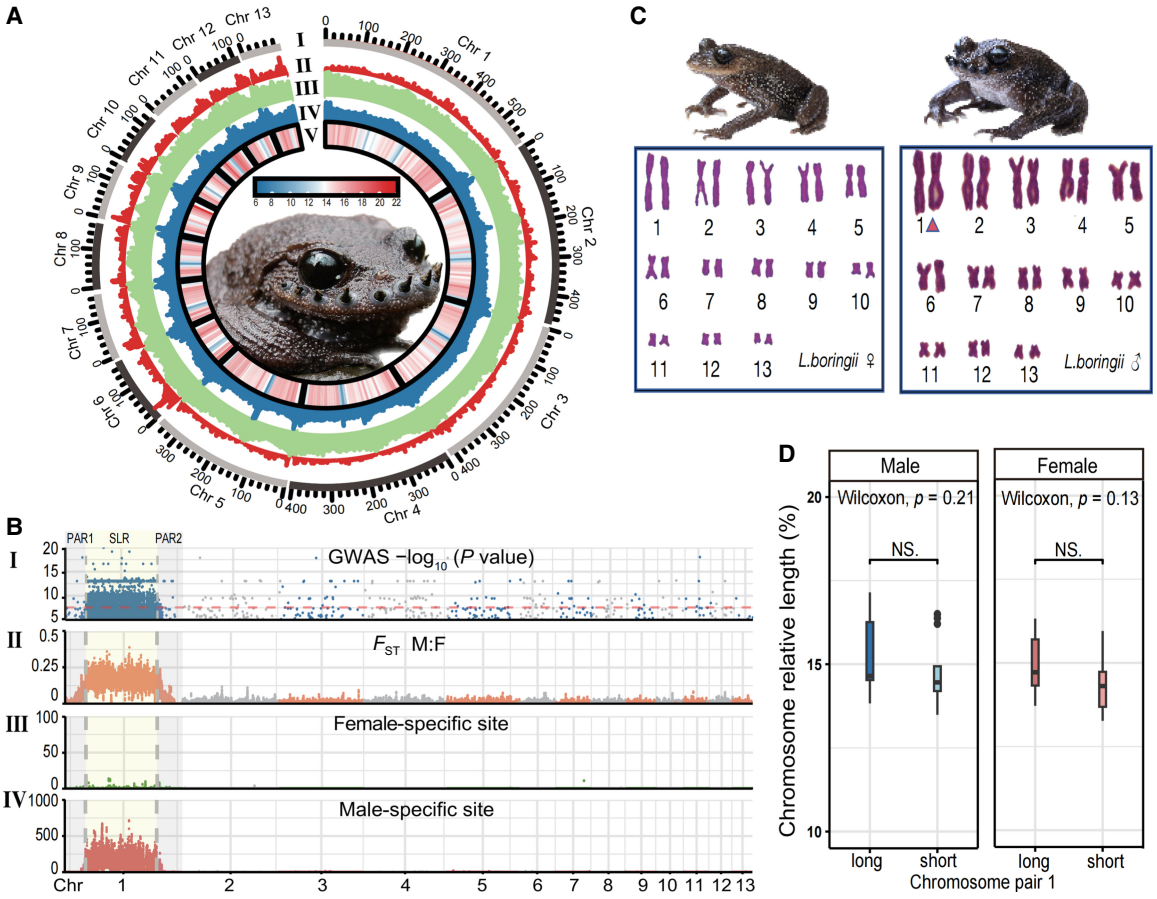

Figure 1. Landscapes of genome assembly (Lbor.v1) and sex chromosomes of *L. boringii*. (*A*) Various metrics calculated in 500 kb sliding windows across each chromosome. From outer to inner: (*I*) sizes of 13 pseudochromosomes; (*II*) gene density; (*III*) repeat sequence distribution; (*IV*) GC content (%); and (*V*) SNP density (numbers of SNP per window). (*B*) Sex-linked regions of *L. boringii*. From *top* to *bottom*: (*I*) $-\log_{10}$ *P*-values of all the significant sex-associated SNPs; (*II*) mean F_{ST}-value between the sexes; (*III*) the number of female-specific sites (heterozygous in females and homozygous in males); and (*IV*) the number of male-specific sites (heterozygous in males and homozygous in females). The red dashed line represents the threshold of GWAS (for statistical details, see Methods), light yellow and gray shadows represent the SLR and two PARs, respectively. (*C*) Karyotype of female (*left* and male (*right*) *L. boringii*. In the male karyotype (2N = 26), the XY pair (Chr 1) marked with a red triangle shows morphological homomorphy. (*D*) Box plots show the comparison of Chr 1 relative length in males (blue) and females (red); *P*-values were based on Wilcoxon rank-sum tests.

genomes. We found that only 6.85% of female-mers were aligned to the Chr 1 of the HapA genome (HAChr 1) and 0.43% to the Chr 1 of the HapB genome (HBChr 1), mainly owing to the inherently low number of female-mers. Meanwhile, 91.89% of Y-mers were aligned to HBChr 1, whereas 7.05% aligned to HAChr 1, indicating HAChr 1 represents the X Chromosome and HBChr 1 represents the Y Chromosome (Fig. 2A; Supplemental Fig. S7; Supplemental Table S17).

We assessed read coverage for both male and female individuals across the sex chromosome in *L. boringii*. No significant difference between sexes was found when comparing coverage based on the XY reference genome (Lbor.v1) with an average $\log_2$(F:M coverage) of −0.067 (Supplemental Fig. S8). We further analyzed HapA and HapB separately and found that in the central region of HBChr 1 (Fig. 2B, light yellow shadow), $\log_2$(F:M coverage) is slightly reduced, consistent with marginally diminished read mapping from female samples compared with males, and therefore, the Y Chromosome contains a small amount of male-specific sequence. In contrast, when comparing the same location on HAChr 1, there was no significant difference in the read coverage between the sexes. Additionally, collinearity analysis did not reveal extensive structural variation between the two haplotypes. We observed only small-scale duplications and inversions in the central region of sex chromosomes (Fig. 2B). These findings suggested high collinearity and similarity between X and Y and implicate that structural variation is not the cause of long SLRs.

To identify the Y-specific region (YSR), we notice there is a smaller interval with pronounced sex differences in coverage within the SLR (Fig. 2B). Specifically, in the YSR spanning ~248 Mb to ~248.95 Mb, $\log_2$(F:M coverage) is substantially male biased (−0.353), whereas the X-specific region (XSR) from ~245.2 Mb to 246.05 Mb shows female-biased coverage (0.433). We further examined the alignment and ultimately pinpointed a 0.84 Mb region spanning 248.14 Mb –248.95 Mb as a strong candidate for the YSR. No protein-coding gene was annotated in this region, and a distinct LTR insertion was detected in the HapB genome (Fig. 2C; Supplemental Fig. S9). One sex-biased gene, *tex15*, in the nearby region (249.95–249.98 Mb) of YSR showed significantly higher expression in adult testes, which provides a potential candidate of sex differentiation (Supplemental Fig. S10).

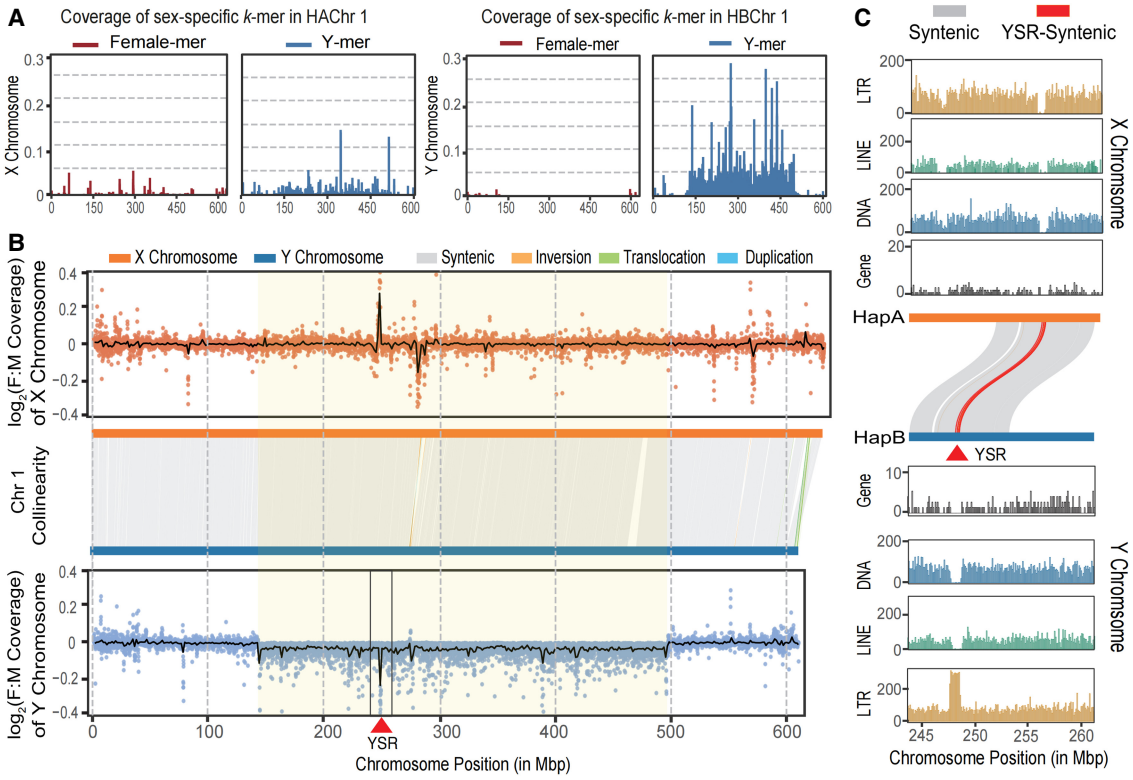

Figure 2. *k*-mer coverage, collinearity, and genomic characteristics of two haploid genomes. (*A*) Coverage of female-mers and Y-mers aligned to two phased Chr 1. The majority of Y-mers were aligned to HBChr 1, with only a small portion of female-mers aligned to either haplotype. (*B*) Collinearity, structural, and $\log_2$(F:M coverage) comparison of HAChr 1 genome (orange) and HBChr 1 genome (blue). The coverage in females was slightly lower than that in males in the central region of HBChr 1 (light yellow shadow), similar to SLR. (*C*) Gene count (dark) and repeat element distribution in haploid genomes (245–260 Mb). Yellow indicates LTR; green, LINE; blue, DNA. The YSR (red triangles) with synteny between HapA and HapB shown in red line.

Chromosome-wide recombination patterns in *L. boringii*

We constructed a high-density genetic map (using the reference genome of Lbor.v1) based on whole-genome resequencing of full-sib samples (Supplemental Data Set S2). After filtering, we mapped a total of 8932 SNPs, of which 4049 were from the dam and 4883 from the sire. Recombination maps allowed the identification of 13 linkage groups in both sexes (Fig. 3A; Supplemental Table S18) and differed between the two parents. The male genetic map was roughly one-third that of the female (1,192.51 cM vs. 3,046.01 cM). These data indicated a significant reduction in male recombination throughout the genome, consistent with extreme heterochiasmy in other frogs (Morescalchi and Galgano 1973; Miura 1994).

By integrating the genetic map with reference genome sequences, we assessed the patterns of recombination across chromosomes. We calculated sex-specific genetic distances and recombination rates. Recombination was largely arrested at the middle region of Chr 1 (from ~85.89 to ~482.56 Mb) in male individuals, indicating a high genetic linkage of that region (Fig. 3B). This low recombination region completely covered the SLR (85.89–482.56 Mb vs. 101.14–450.89 Mb), indicating that the ultralong SLR may be largely attributed to the evolution of the male-determining factor in a region of ancestrally low male recombination.

Homomorphic sex chromosomes can be maintained by occasional XY recombination events, which prevents divergence and degeneration of the Y Chromosome (Stöck et al. 2013; Rodrigues et al. 2018; Ping et al. 2022). Guerrero et al. (2012) demonstrated a male–female ratio of recombination rates as low as 10^{-5} could maintain sex chromosome homomorphy. Because recombination follows phenotypic sex, rather than genotypic sex in vertebrates (Rodrigues et al. 2018), XY recombination likely occurs in sex-reversed XY females. To quantify the potential XY recombination in sex-reversed females and determine whether it is sufficient to explain sex chromosome homomorphy in *L. boringii*, we determined the proportion of XY females. Genotypic sex was distinguished using Sanger sequencing of four sex-specific sites we identified above (Fig. 1D, track IV; Supplemental Tables S19, S20; Supplemental Fig. S11). We observed a relatively high proportion of sex-reversed XY females: out of 97 phenotypic females, eight individuals exhibited a putative XY genotype (8.2%). In contrast, no XX phenotypic males out of 73 were found (Fig. 3C; Supplemental Data Set S3). Our data indicate an average female SLR recombination rate of about 0.82 (Fig. 3C; Supplemental Data Sets S4, S5), and based on this, we estimated the recombination rates in males in *L. boringii* to be about 0.0672, far greater than the minimum threshold suggested by Guerrero et al. (2012). This indicates that the recombination rates in males are sufficient to preserve homomorphic sex chromosomes and minimize XY differentiation.

Sex-biased and allele-specific expression

Sex-linked genes may exhibit different gene expression patterns between the sexes for two reasons. First, degeneration of the Y

Chromosome may produce dose differences, with greater expression in females in the absence of dosage compensation (Mank 2013). Additionally, the unique inheritance pattern of the X and Y can lead to sexualization of gene expression independent of dosage compensation (Rice 1984; Connallon and Knowles 2005; Mank 2009), To determine whether the sex chromosomes of the Emei moustache toad exhibit significant sex-biased expression, we compared transcriptome data (reference genome: Lbor.v1) from gonads in two sexes at four critical sexual differentiation stages (Gosner stages: G25, G28, G42, and adult) (Supplemental Data Set S6; Supplemental Fig. S12). After multiple-test correction, with differential fold change ($|FC|$) ≥ 2 and false-discovery rate (FDR) ≤ 0.05, 14,217 transcripts (out of 20,327) were significantly sex biased in expression in at least one of the four developmental stages (Supplemental Data Set S7). The number of sex-biased genes increased drastically after the stage G25 when the gonads first became histologically distinct from each other (Fig. 4A; Supplemental Fig. S12).

To investigate possible dose effects of the X Chromosome and sexualization of gene expression, we compared sex-biased gene expression across genomic regions. We observed significant differences in expression between the SLR and autosomes in the gonad, with both more male- and female-biased genes, but no differences in somatic tissues (Fig. 4B,C; Supplemental Data Set S8). More importantly, we only found evidence of mild allele-specific expression (ASE) of sex chromosomes in male gonads but not in other tissues ($P_{Mgonad} = 0.041$, $P_{Msoma} = 0.52$, $P_{Fgonad} = 0.67$, $P_{Fsoma} = 0.14$, Wilcoxon rank-sum test) (Fig. 4D; Supplemental Fig. S13), indicating the Y Chromosome has a certain regulatory effect on the gonads, but without Y degeneration or X gene dose effects. Overall, we observed modest evidence of sexualization of gene content of sex chromosomes but no evidence of reduced gene activity on the Y Chromosome.

Candidate sex-differentiation genes in *L. boringii*

The SLR likely contains the sex determining locus. Thus, we identified sex-linked genes in the SLR with at least one male-specific missense SNP, resulting in 395 genes with at least one heterozygous missense mutation in males (Supplemental Data Set S9). Heatmap and hierarchical clustering analysis performed on differentially expressed sex-linked genes (FDR < 0.05) in gonad tissues revealed that samples clustered by sex rather than by developmental stage (Fig. 5A). Three candidate genes, *zp3*, *pgam5*, and *c8h9orf78*, exhibit high expression in the ovary in both later development stages and have been implicated in vertebrate female development. Two genes, *ptgr1* and *cirbp*, exhibit high expression in the testis and have conserved roles in vertebrate gonadogenesis. These five genes might participate in the process of development of sex differentiation, especially given their sex-specific expression in the developing gonads (Supplemental Fig. S14).

To further identify key genes and pathways that regulate gonadal development or differentiation, we analyzed the gene coexpression networks and identified genetic modules by weighted gene correlation network analysis (WGCNA) (Langfelder and Horvath 2007). This method can identify core sex-related pathways and genes that play an important role in transcription regulation and predict gene regulatory relationships. WGCNA revealed that the expression genes of female and male gonads can be clustered into 20 modules (Fig. 5B; Supplemental Table

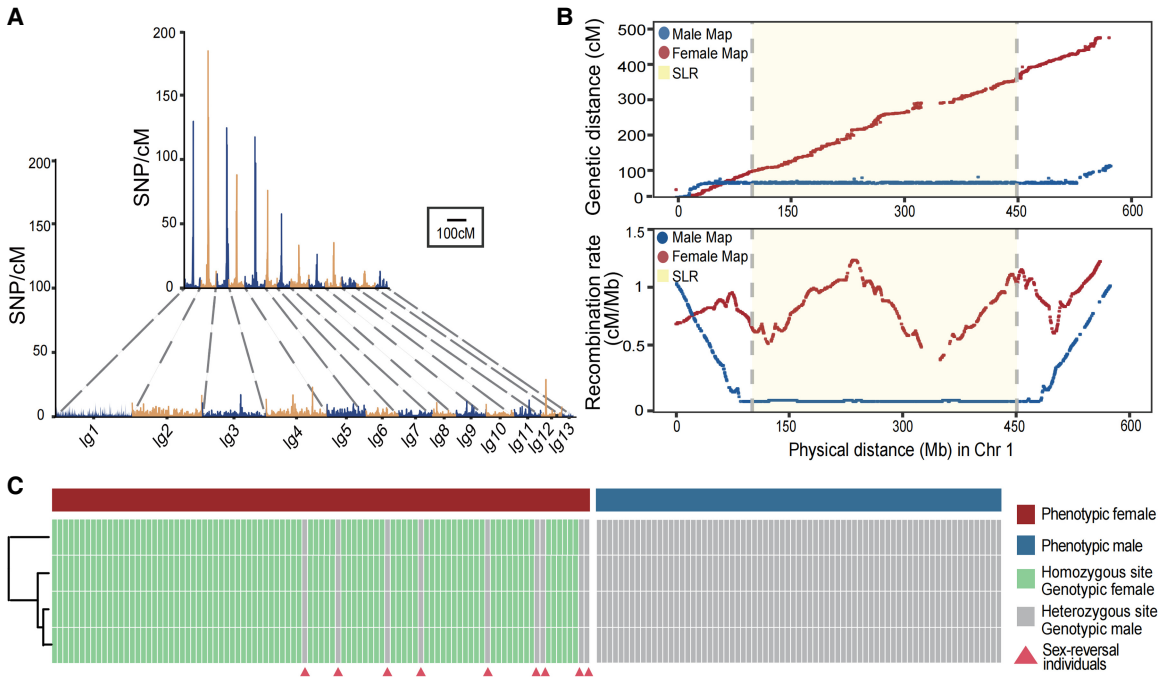

Figure 3. Genetic linkage map and recombination of *L. boringii*. (*A*) SNP density along the male (*top*) and female (*bottom*) recombination maps. (*B*) Concordance of physical SNP marker positions on reference genome with the genetic linkage map. The *x*-axis represents the physical position (Mb) of markers, the *y*-axis represents the genetic positions (cM) of markers on the linkage map (*top*) and the recombination rates (*bottom*); the light yellow region represents the position of the SLR identified from the GWAS result. (*C*) Sex-reversed individuals of *L. boringii*. The *top* row corresponds the phenotypic sex of *L. boringii* (blue indicates male individuals; red, female individuals), and other rows correspond to results of sex-linked markers: heterozygous in all genotypic males and homozygous in genotypic females. Individuals whose phenotypic and genotypic sex did not match were indicated as sex reversals (red triangles).

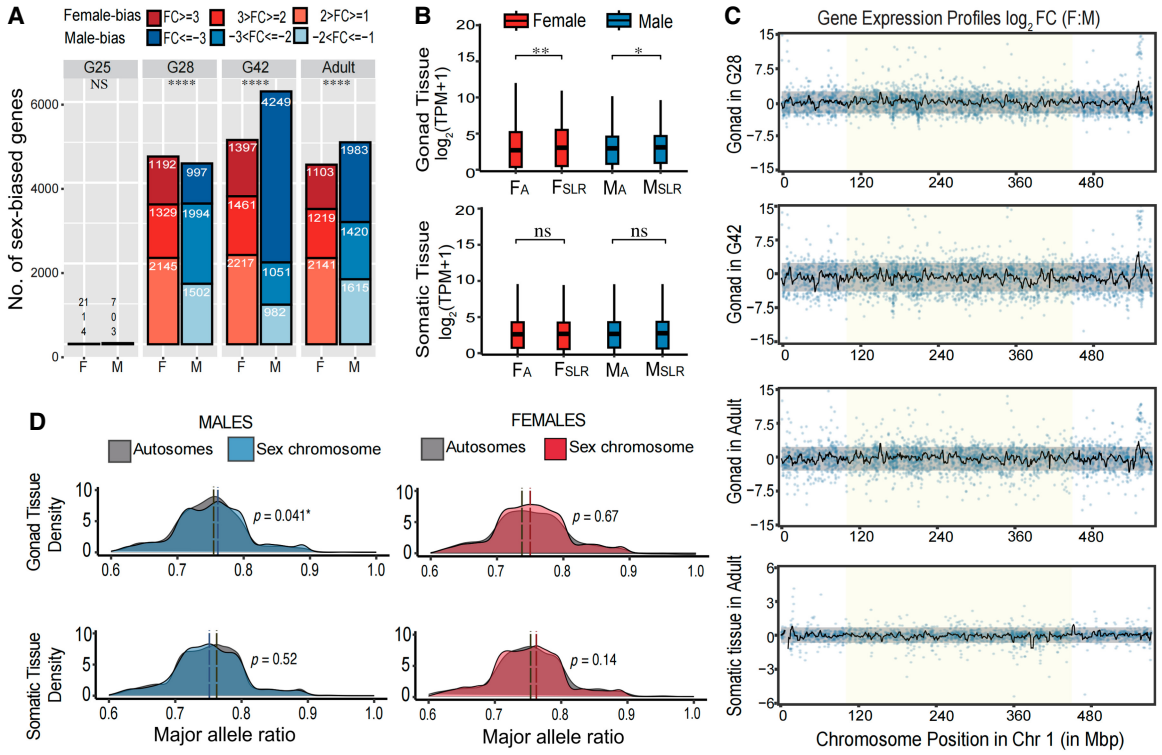

Figure 4. Patterns of gene expression and ASE. (*A*) Sex-biased gene expression in gonads across developmental stages in *L. boringii*. Sex-biased genes were classified into three categories by $\log_2$ FC (F:M), in which negative values indicate male-biased genes, and positive values indicate female-biased genes. (*B*) Comparison of gene expression between autosomes (A) and SLR in males (blue) and females (red). (*C*) Comparison of sex chromosome gene expression between the sexes across a three-development stage of gonad tissue and somatic tissue from adults. Sex chromosomes lack sex-biased expression beyond the expression range of autosomes (gray shading, the 95% confidence intervals based on bootstrapping), including the SLR (yellow shading). (*D*) Density plots show the distribution of the major allele frequency of autosomes (gray) and sex chromosomes (blue in male and red in female) genes in the two sexes. Vertical dotted lines indicate median values, and *P*-values are based on Wilcoxon rank-sum tests.

S21). Of these modules, the Me07 ($r = 0.712$, $P < 0.001$, Fig. 5B) and Me09 ($r = 0.702$, $P < 0.001$, Fig. 5B) modules were significantly positively correlated with sex. To better understand the function of these genes, we separately conducted the KEGG enrichment (Fig. 5C) for genes from four groups, namely, genes in the Me07 module, genes in the Me09 module, genes having missense mutations (MMs genes), and the sex-link genes (SL genes, located in the SLR). The PI3K-Akt signaling pathway was significantly enriched in all four gene sets (Fig. 5C; Supplemental Data Sets S10–S13), supporting its crucial role in the gonadal development or differentiation. Consistently, this pathway has been found to play a critical role in oocyte-induced primordial follicle activation (Castrillon et al. 2003; Reddy et al. 2008).

Discussion

In this study, we built a highly contiguous reference genome of *L. boringii* and identified a long SLRs (~350 Mb), comprising >60% of Chr 1. This is among the largest SLRs identified in vertebrates and the largest thus far in anurans. For comparison, one of the largest SLRs in fish, the "giant" sex chromosomes in several tilapia, is ~105 Mb (77.6% of LG3)(Conte et al. 2021). The SLR in humans, which exhibits extensive heteromorphy, is 153.08 Mb (Ross et al. 2005). The SLR in *Xenopus* ranges from 10.7 Mb (7.71% of Chr 7) in *Xenopus tropicalis* (Furman et al. 2020a) to 54.1 Mb (44.17% of Chr 8L) in *Xenopus borealis* (Song et al. 2021; Evans et al. 2022).

Our study revealed that the extensive SLR of Chr 1 in *L. boringii* exhibits significant allele frequency differences between the X and Y Chromosomes, yet still retains high collinearity and similarity, suggesting little large-scale genetic differentiation or degeneration of the Y Chromosome. Large-scale inversions are often thought to catalyze recombination suppression between the X and Y Chromosomes (Charlesworth et al. 2005), although there is little direct evidence of this, and other mechanisms have been proposed (Iwase et al. 2003; Natri et al. 2013; Furman et al. 2020b). High collinearity and similarity between X and Y haplotypes implicate a pre-existing pattern of low recombination itself, likely predating the origin of Chr 1 as the sex chromosomes, rather than structural variation, in sex chromosome formation.

In addition to Chr 1, the sexually different recombination pattern also exists in other pseudochromosomes (Fig. 3A; Supplemental Figs. S15, S16). This pattern of strongly sex-biased recombination, with male recombination restricted to the end of the chromosome, offers some important clues. In animals, males and females often experience different rates of total (Conte et al. 2021) and fine-scale (Sardell and Kirkpatrick 2020) recombination. Many anurans exhibit strong sex-biased recombination (Rodrigues et al. 2013; Brelsford et al. 2016b,c; Furman and Evans 2018; Dufresnes et al. 2021), with chromosomes only paired at their terminal region during male meiosis (Morescalchi and Galgano 1973; Miura 1994), similar to what we observed in *L. boringii*. Genomic regions with sex-specific recombination rates may be important in sex chromosome divergence (Wright et al. 2016), and our results

suggest that the low rate of male recombination in the interior region of the chromosomes predates the origin of the SLR. This in turn would lead to large regions quickly becoming sex-linked owing to pre-existing low recombination in males. Thus, we argue that this extensive SLR did not evolve by recombination suppression after the acquisition of new sex-determining genes but by the ancestral nature of the low crossover rates in males.

Sex reversal, as we observed in *L. boringii*, is common among anurans (Perrin 2009; Stöck et al. 2011; Rodrigues et al. 2018), poikilothermic vertebrates (e.g., medaka and tilapia), and even endotherms like the mouse (Kondo et al. 2001; Lynn et al. 2005; Campos-Ramos et al. 2009). Sex reversal induces a nonzero recombination rate (about 0.0672) in the SLR of male *L. boringii*. Similarly, X–Y recombination in *Hyla* spp. is low (10^{-5} times lower than X–X) but nonzero, suggesting such low recombination maintains sex chromosome homomorphy (Guerrero et al. 2012), explaining the coexistence of extreme heterochiasmy and homomorphic sex chromosomes in *L. boringii*. In many cases, frog species maintain homomorphic sex chromosomes for more than 100 million years (Ma and Veltsos 2021), with very limited differentiation between the sex chromosomes in the heterogametic sex (Stöck et al. 2011, 2013; Furman et al. 2020b). This may explain why heteromorphic sex chromosomes are relatively scarce in the clade (Busin et al. 2008; Schmid et al. 2012; Schartl et al. 2016). In summary, our results show ancestral low-recombination regions in male individuals coupled with occasional sex reversal events have formed a long-term balance, enabling the *L. boringii* to maintain homomorphic sex chromosomes.

The location of sex chromosomes among anurans is nonrandom (Miura 2017; Jeffries et al. 2018), and Chr 1 is more often the sex chromosome than expected by chance (Brelsford et al. 2013; Dufresnes et al. 2015; Jeffries et al. 2018). Although the presence of key male-determining genes in vertebrates, such as *Amh*, *Dmrt1*, and *Irf9* (Adolfi et al. 2021), on this chromosome make it possible the repeated independent origin of sex chromosomes on Chr 1, an arguably more parsimonious explanation is that Chr 1 represents the ancestral sex chromosomes of anurans. From the synteny of anuran genomes, Chr 1 is highly conserved with almost no fusion events from other chromosomes (Bredeson et al. 2024; Kosch et al. 2025). The syntenic region corresponding to Chr 1 has repeatedly evolved into sex chromosomes in multiple vertebrate species (Montiel et al. 2016). More importantly,

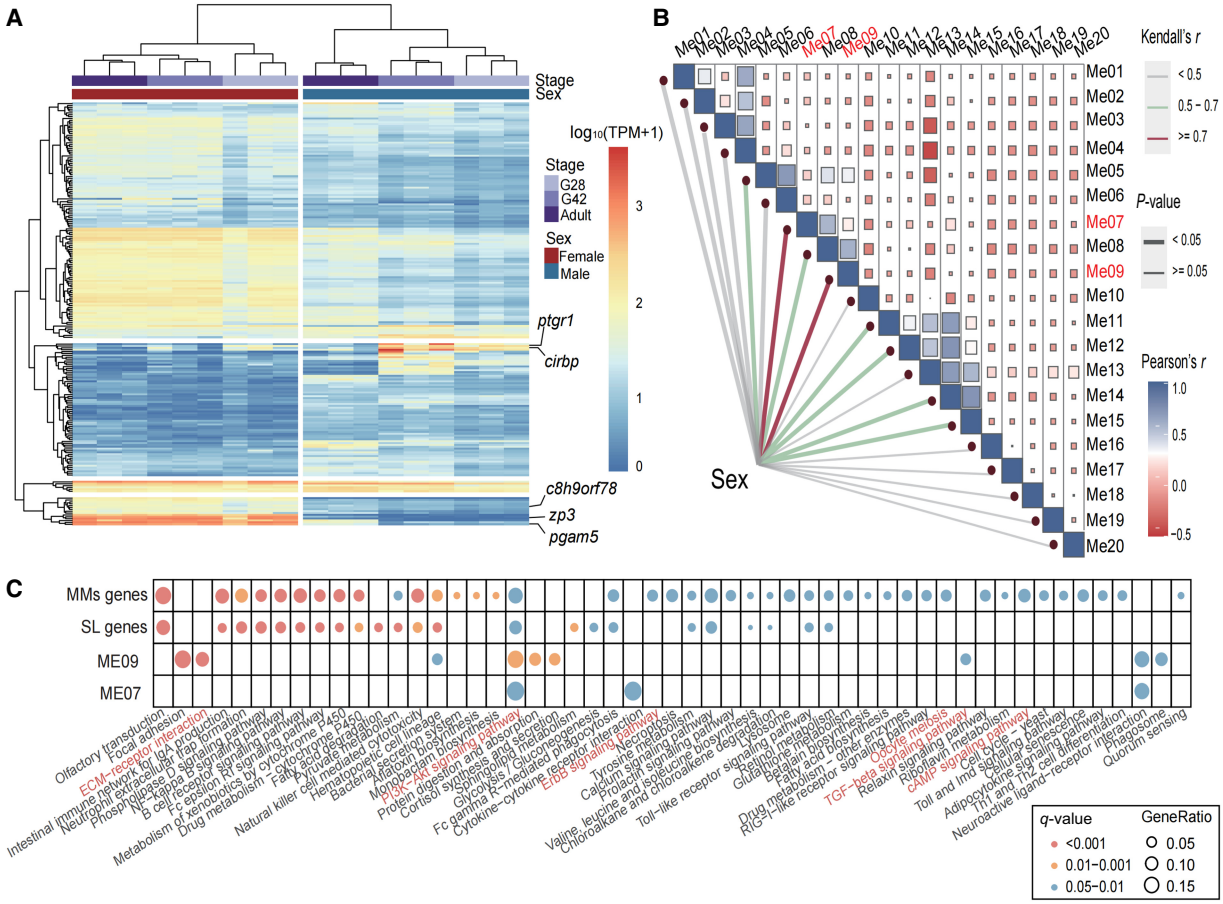

Figure 5. Candidate genes and pathways correlated with sex development and differentiation in *L. boringii*. (*A*) Heatmap and the hierarchical clustering of SL gene expression from gonad tissues in three late development stages (G28, G42, Adult). Five candidate genes (*zp3*, *pgam5*, *c8h9orf78*, *ptgr1*, and *cirbp*) exhibiting high sex-specific expression across multiple periods are labeled in the heatmap. (*B*) Two key modules are highly correlated with sex (Kendall's $r > 0.7$, $P < 0.05$). Rows and columns correspond to modules, and each cell represents the corresponding correlation (Pearson's *r*) of module to module. The color and thickness of the lines represent the correlation (Kendall's *r*) and significance (*P*-value) between sex and modules. (*C*) KEGG functional enrichment of genes with genetic differences (MM genes and SL genes) and expression differences (Me07 and Me09 modules).

L. boringii is a member of the *Leptobrachium* genus, which diverged roughly 46.4 million years ago (31.6–61.4 million years ago) (Matsui et al. 2010; Li et al. 2023) and belongs to Archaeobatrachia suborder (Feng et al. 2017). Given the phylogenetic position of *Leptobrachium* and the prevalence of Chr 1 as the sex chromosome in anurans, it may represent the ancestral sex chromosome pair in Anura.

Many animal sex chromosomes exhibit proportionally greater or fewer sex-biased genes than expected by chance (for summary, see Dean and Mank 2014), which may be related to sexual selection and conflict arising from mating systems. Some amphibians with heteromorphic sex chromosomes (e.g., *Engystomops*) exhibit sexual dimorphism and parental care (Elinson and del Pino 2012). These unique life history traits, combined with sexual selection, may enhance the effects of sex-biased genes. *L. boringii* has strong male-biased sexual size dimorphism, unique keratinized nuptial spines, and male-specific parental care (Zhang et al. 2016), suggesting sexual selection in the species that might lead to sexualization of gene expression within the SLR. However, we observed a mild enrichment of both ASE expression in testes and male- and female-biased SLR genes in the gonad but not somatic tissue (Fig. 4). These conclusions suggest that occasional XY recombination may hinder sexualization of gene regulation in *L. boringii*.

Finally, we identified five potential candidate genes on Chr 1 that are involved in gonad development and differentiation. *zp3* is critical in the process of sperm—egg interaction in African clawed frogs (Omata and Katagiri 1996; Vo and Hedrick 2000). The overexpression of *pgam5* can negatively affect the cumulus cells by increasing mitochondrial fission (Li et al. 2022). In humans, *C9orf78* (ortholog of *c8h9orf78*) deletion can lead to XY individuals with female phenotypes (Veitia et al. 1997) and is a candidate gene for ovarian dysgenesis (Ledig et al. 2010). *ptgr1* encodes a Sertoli cell–specific prostaglandin catabolic enzyme (Tai et al. 2002; Shima et al. 2004) and has a possible role in prostaglandin or other eicosanoid signaling (Fahrioglu et al. 2007). *cirbp* mediates temperature effects on the developing gonads in snapping turtles (*Chelydra serpentina*) (Schroeder et al. 2016). Except for the PI3K-Akt signaling pathway, other pathways may also play significant roles in gonad development, such as the TGF-β signaling pathway, ErbB signaling pathway, and oocyte meiosis, all of which have been proven to be involved in diverse signaling pathways with known regulatory roles in gonad development (Malki et al. 2005; Prevot et al. 2005; Rutkowska and Badyaev 2008; Pan et al. 2021; Wu et al. 2024).

All evidence taken together, we identified a homomorphic yet large SLR on Chr 1 of *L. boringii*; the X and Y Chromosomes showed little differences in gene content, collinearity, and size, with modest sexualization, as demonstrated both in genetic and karyotype analysis. We propose that sex-determining genes originating in regions of extreme heterochiasmy and low recombination drive SLR expansion. The low recombination regions on the Y Chromosome form an equilibrium with the XY recombination of sex-reversed individuals, which resulted in a long-term suppression of XY divergence. In this case, Chr 1 may have been maintained as the sex chromosome for a long evolutionary period of time. Additionally, repeated recruitment of Chr 1 as a sex chromosome in frogs (Miura 2017; Jeffries et al. 2018) suggests it is likely the ancestral sex chromosome in amphibians. Our findings highlight the force of X–Y recombination to maintain homomorphic sex chromosome and offer insights into the origin and persistence of amphibian sex chromosomes.

Methods

Sample collection

L. boringii samples were collected from the Badagongshan National Nature Reserve, China. Muscle and liver tissues from one male were used for genomic sequencing; whole-body tissues, for transcriptomic sequencing and gene structural annotation. Liver tissue from another male was used for Hi-C and HiFi library construction. Whole-genome resequencing involved 40 individuals and one full-sib family. Transcriptomic sequencing used gonads at four developmental stages and adult somatic tissues. All procedures complied with CCNU-IACUC-2022-010 and relevant ethical regulations. Details for DNA/RNA extraction and sequencing are in the Supplemental Methods.

Genome sequencing, assembly, and annotation

The *L. boringii* genome was assembled using Illumina (329.7 Gb, about 97.5× coverage), PacBio (333.6 Gb, about 98.6× coverage), and Hi-C sequencing (173.6 GB, about 51.4× coverage). Draft assembly was generated using Canu v2.0 (Koren et al. 2017) and WTDBG v1.1.006 (https://github.com/ruanjue/wtdbg), followed by polishing and de-redundancy processes. Genome completeness was assessed by BUSCO v4.0.1 (Simão et al. 2015). Contigs were anchored into chromosomes using Juicer v1.5 (Durand et al. 2016) and 3D-DNA v180922 (Dudchenko et al. 2017), yielding a 3.38 Gb *L. boringii* reference genome (Lbor.v1). Transposable elements (TEs) were annotated using RepeatMasker, RepeatProteinMask (http://www.repeatmasker.org), RepeatModeler (Flynn et al. 2020), and LTR-FINDER (Castelo et al. 2002). Protein-coding genes were annotated using a combination of de novo prediction, homology search, and transcript-based assembly, utilizing tools like GlimmerHMM v3.0.4 (Majoros et al. 2004), AUGUSTUS v3.3.2 (Stanke et al. 2006), and MAKER2 v2.31.10 (Holt and Yandell 2011). Gene functions were assigned using several databases (Supplemental Methods) and assessed with BUSCO v4.0.1 (Simão et al. 2015). For detailed downstream analyses, see the Supplemental Methods.

Cytogenetic karyotype analysis

Metaphase chromosomes were prepared from *L. boringii* tadpole kidneys using a modified version of the method from Phimphan and Aiumsumang (2021). For detailed adaptations, see the Supplemental Methods. Metaphase chromosomes were examined and photographed, and various metrics were calculated. Differences in relative length (RL) of Chr 1 between sexes were assessed using the Wilcoxon rank-sum test.

Variant calling and primary data filtration

Raw Illumina data were quality-checked using FastQC v0.11.5 (https://www.bioinformatics.babraham.ac.uk/projects/fastqc/), mapped to the reference genome with BWA (Li and Durbin 2009), and processed with SAMtools v1.9 (Li et al. 2009) and Picard (version 2.1; http://broadinstitute.github.io/picard/) for sorting and duplicate removal. Variants were called using GATK v.3.8 (McKenna et al. 2010) and filtered based on standard criteria (for details, see Supplemental Methods).

Identification of sex chromosomes and the SLR

GWAS using EMMAX (Kang et al. 2010) identified the SLR, with a significance threshold of $P = 2.699 \times 10^{-8}$ (dividing 0.05 by the number of total SNP). F_{ST}-values between males and females were calculated using 200 kb sliding windows. The top 1% was

selected as the significance threshold of F_{ST}. The sex-specific SNPs were filtered and defined based on allele frequency differences (see Supplemental Methods). We identified 274,384 male-specific SNPs, 240 female-specific SNPs, and 607 missense variants belonging to 395 genes by SnpEff (Cingolani et al. 2012) for variant annotation.

Haploid genome, *k*-mer analysis, and coverage

We supplemented PacBio HiFi data with additional CCS reads (166.03 Gb, ~49.1× coverage) from a male *L. boringii* and assembled two haploid genomes using hifiasm (https://github.com/chhylp123/hifiasm) and HiCanu (Nurk et al. 2020). Hi-C-based refinement yielded two haploid genomes, one of which was 3.923 Gb (HapA) and the other 3.740 Gb (HapB), with completeness assessed by BUSCO v4.0.1 (Simão et al. 2015).

Y Chromosome identification followed the *k*-mer analysis method (Morris et al. 2018) using the HAWK pipeline (Rahman et al. 2018) on paired-end DNA-seq reads. The sex-specific *k*-mers were identified, filtered (see Supplemental Methods), and aligned to haploid genomes to infer the Y Chromosome.

We aligned male and female reads to the HapA and HapB reference genomes using BWA-MEM v0.7.17 (Li and Durbin 2009) and calculated male-to-female coverage ratios and unmapping reads (HapA: 0.264% in females and 0.203% in males; HapB: 0.374% in females and 0.303% in males) (Supplemental Table S16). Synteny between HAChr 1 and HBChr 1 was analyzed by minimap2 v2.24 (Li 2018) and structural variants by SyRI v1.6 (Goel et al. 2019), and syntenic blocks >20 kb were plotted using plotsr v0.5.4 (Goel and Schneeberger 2022).

High-density genetic map

Markers were encoded as lm × ll (male heterozygous, female homozygous) and nn × np (male homozygous, female heterozygous). After applying four filtering criteria to exclude noninformative loci (Supplemental Methods), a total of 10,884 markers (5878 lm × ll and 5006 nn × np) were retained. We used Lep-MAP3 (Rastas 2017) to partition linkage groups (LOD threshold 3) and MareyMap (Siberchicot et al. 2017) for postprocessing, generating a genetic map with 13 linkage groups. Recombination rates were estimated using a LOESS model (span = 0.2), calculating local recombination rates (cM/Mb) from the relationship between physical and genetic positions.

Validation of sex-specific markers by conventional Sanger sequencing

Sex-linked SNPs were verified by designing primers from 300 bp flanking sequences. Four primer pairs were confirmed as heterozygous in 24 males and homozygous in 24 females by Sanger sequencing (Supplemental Methods; Supplemental Fig. S11; Supplemental Tables S19, S20). These markers accurately determine genotypic sex in *L. boringii* for sex reversal and RNA sequencing.

RNA sequencing and gene expression analysis

Histological analysis identified four key stages of sex differentiation: (1) G25, undifferentiated gonads; (2) G28, identifiable gonads; (3) G42, mature gonads at metamorphosis peak; and (4) adult, sexually mature (Supplemental Fig. S12). Gonad and somatic tissues from both sexes at these stages were collected. We confirmed that the phenotypic and genotypic sex were consistent by Sanger sequencing (Supplemental Table S19, S20) to exclude sex-reversed individuals.

Standard methods were used for total RNA extraction, which was sequenced from three biological replicates at each stage and sex (Supplemental Methods). Reads were mapped to our reference genome of Lbor.v1 and two haploid genomes (Supplemental Fig. S17) using HISAT2 (Kim et al. 2015), and differential expression was analyzed using edgeR (Robinson et al. 2010) and DESeq2 (Love et al. 2014), applying $|FC| \geq 2$ and FDR ≤ 0.05. Sex-biased genes were also defined by $|FC| \geq 2$ and FDR ≤ 0.05 and classified by |FC| as low (two to four), mid (four to eight), and high (greater than eight), following the method of Montgomery and Mank (2016) to reduce bias from whole-body sampling.

ASE analysis

ASE patterns were estimated using modified pipelines (Quinn et al. 2014), and the detailed modifications are shown in the Supplemental Methods. Briefly, SNPs were called separately for males and females using SAMtools mpileup v1.9 (Li et al. 2009) and filtered with VarScan (Koboldt et al. 2012). To mitigate reference allele mapping bias (Stevenson et al. 2013), we used the method of Zimmer et al. (2016), excluding clusters of more than five SNPs within 100 bp windows and setting a coverage filtering threshold.

ASE was tested using a two-tailed binomial test ($P < 0.05$) with multiple testing correction for filtered SNPs. Genes were classified as ASE based on read ratio thresholds (≥70% allele bias) (Supplemental Methods). Significant differences in ASE patterns between sexes and chromosomes were tested using Wilcoxon rank-sum tests.

Gene coexpression analysis

Coexpression analysis was performed on 24 samples using WGCNA v1.63 (Langfelder and Horvath 2007). For each module, KEGG enrichment was conducted to understand the gene module function. WGCNA and KEGG enrichment processing and analysis were described in the Supplemental Methods.

Data access

The raw sequencing data generated in this study have been submitted to the NCBI BioProject database (https://www.ncbi.nlm.nih.gov/bioproject/) under accession number PRJNA1108069.

Competing interest statement

The authors declare no competing interests.

Acknowledgments

This work was supported by the National Natural Science Foundation of China (no. 32270459) and the National Key Research and Development Program of China (2023YFF1304800). J.E.M. acknowledges support from the Natural Sciences and Engineering Research Council of Canada and a Canada 150 Research Chair.

Author contributions: S.X. and H.W. designed the original concept and scientific objectives. S.X. designed experiments, analyzed the data, and wrote the manuscript. J.L. assembled and updated the reference genome, evaluated the results, and revised the manuscript. W.C. conducted karyotype experiments. L.J.M.F., C.H., Y.F., and Q.A. assisted with getting samples and processing bioinformatics. M.Z. critically reviewed the paper. J.E.M. contributed critical insights to the design and supervised research and reviewed the paper. H.W. obtained funding and other resources, supervised all research, and reviewed the paper.

References

Adolfi MC, Herpin A, Schartl M. 2021. The replaceable master of sex determination: bottom-up hypothesis revisited. *Phil Trans R Soc* **376:** 20200090. doi:10.1098/rstb.2020.0090

Alho JS, Matsuba C, Merilä J. 2010. Sex reversal and primary sex ratios in the common frog (*Rana temporaria*). *Mol Ecol* **19:** 1763–1773. doi:10.1111/j.1365-294X.2010.04607.x

Almeida P, Sandkam BA, Morris J, Darolti I, Breden F, Mank JE. 2021. Divergence and remarkable diversity of the Y chromosome in guppies. *Mol Biol Evol* **38:** 619–633. doi:10.1093/molbev/msaa257

Bachtrog D, Hom E, Wong KM, Maside X, de Jong P. 2008. Genomic degradation of a young Y chromosome in *Drosophila miranda*. *Genome Biol* **9:** R30. doi:10.1186/gb-2008-9-2-r30

Bachtrog D, Mank JE, Peichel CL, Kirkpatrick M, Otto SP, Ashman T-L, Hahn MW, Kitano J, Mayrose I, Ming R, et al. 2014. Sex determination: why so many ways of doing it? *PLoS Biol* **12:** e1001899. doi:10.1371/journal.pbio.1001899

Bellott DW, Hughes JF, Skaletsky H, Brown LG, Pyntikova T, Cho T-J, Koutseva N, Zaghlul S, Graves T, Rock S, et al. 2014. Mammalian Y chromosomes retain widely expressed dosage-sensitive regulators. *Nature* **508:** 494–499. doi:10.1038/nature13206

Bellott DW, Skaletsky H, Cho T-J, Brown L, Locke D, Chen N, Galkina S, Pyntikova T, Koutseva N, Graves T, et al. 2017. Avian W and mammalian Y chromosomes convergently retained dosage-sensitive regulators. *Nat Genet* **49:** 387–394. doi:10.1038/ng.3778

Bredeson JV, Mudd AB, Medina-Ruiz S, Mitros T, Smith OK, Miller KE, Lyons JB, Batra SS, Park J, Berkoff KC, et al. 2024. Conserved chromatin and repetitive patterns reveal slow genome evolution in frogs. *Nat Commun* **15:** 579. doi:10.1038/s41467-023-43012-9

Brelsford A, Stöck M, Betto-Colliard C, Dubey S, Dufresnes C, Jourdan-Pineau H, Rodrigues N, Savary R, Sermier R, Perrin N. 2013. Homologous sex chromosomes in three deeply divergent anuran species. *Evolution (N Y)* **67:** 2434–2440. doi:10.1111/evo.12151

Brelsford A, Dufresnes C, Perrin N. 2016a. High-density sex-specific linkage maps of a European tree frog (*Hyla arborea*) identify the sex chromosome without information on offspring sex. *Heredity (Edinb)* **116:** 177–181. doi:10.1038/hdy.2015.83

Brelsford A, Dufresnes C, Perrin N. 2016b. *Trans*-species variation in *Dmrt1* is associated with sex determination in four European tree-frog species. *Evolution (N Y)* **70:** 840–847. doi:10.1111/evo.12891

Brelsford A, Rodrigues N, Perrin N. 2016c. High-density linkage maps fail to detect any genetic component to sex determination in a *Rana temporaria* family. *J Evol Biol* **29:** 220–225. doi:10.1111/jeb.12747

Brelsford A, Lavanchy G, Sermier R, Rausch A, Perrin N. 2017. Identifying homomorphic sex chromosomes from wild-caught adults with limited genomic resources. *Mol Ecol Resour* **17:** 752–759. doi:10.1111/1755-0998.12624

Bull JJ. 1983. *Evolution of sex determining mechanisms*. Benjamin/Cummings, San Francisco.

Busin CS, Andrade GV, Bertoldo J, Del Grande ML, Uetanabaro M, Recco-Pimentel SM. 2008. Cytogenetic analysis of four species of *Pseudis* (Anura, Hylidae), with the description of ZZ/ZW sex chromosomes in *P. tocantins*. *Genetica* **133:** 119–127. doi:10.1007/s10709-007-9189-7

Campos-Ramos R, Harvey SC, Penman DJ. 2009. Sex-specific differences in the synaptonemal complex in the genus *Oreochromis* (Cichlidae). *Genetica* **135:** 325–332. doi:10.1007/s10709-008-9280-8

Carpentier F, Rodríguez de la Vega RC, Branco S, Snirc A, Coelho MA, Hood ME, Giraud T. 2019. Convergent recombination cessation between mating-type genes and centromeres in selfing anther-smut fungi. *Genome Res* **29:** 944–953. doi:10.1101/gr.242578.118

Castelo AT, Martins W, Gao GR. 2002. TROLL—tandem repeat occurrence locator. *Bioinformatics* **18:** 634–636. doi:10.1093/bioinformatics/18.4.634

Castrillon DH, Miao L, Kollipara R, Horner JW, DePinho RA. 2003. Suppression of ovarian follicle activation in mice by the transcription factor Foxo3a. *Science* **301:** 215–218. doi:10.1126/science.1086336

Charlesworth B. 1991. The evolution of sex chromosomes. *Science* **251:** 1030–1033. doi:10.1126/science.1998119

Charlesworth B, Charlesworth D. 2000. The degeneration of Y chromosomes. *Phil Trans R Soc Lond B* **355:** 1563–1572. doi:10.1098/rstb.2000.0717

Charlesworth D, Charlesworth B, Marais G. 2005. Steps in the evolution of heteromorphic sex chromosomes. *Heredity (Edinb)* **95:** 118–128. doi:10.1038/sj.hdy.6800697

Cingolani P, Platts A, Wang LL, Coon M, Nguyen T, Wang L, Land SJ, Lu X, Ruden DM. 2012. A program for annotating and predicting the effects of single nucleotide polymorphisms, SnpEff: SNPs in the genome of *Drosophila melanogaster* strain w1118; iso-2; iso-3. *Fly (Austin)* **6:** 80–92. doi:10.4161/fly.19695

Connallon T, Knowles LL. 2005. Intergenomic conflict revealed by patterns of sex-biased gene expression. *Ttrends Genet* **21:** 495–499. doi:10.1016/j.tig.2005.07.006

Conte MA, Clark FE, Roberts RB, Xu L, Tao W, Zhou Q, Wang D, Kocher TD. 2021. Origin of a giant sex chromosome. *Mol Biol Evol* **38:** 1554–1569. doi:10.1093/molbev/msaa319

Cortez D, Marin R, Toledo-Flores D, Froidevaux L, Liechti A, Waters PD, Grützner F, Kaessmann H. 2014. Origins and functional evolution of Y chromosomes across mammals. *Nature* **508:** 488–493. doi:10.1038/nature13151

Dai W, Mank JE, Ban L. 2024. Gene gain and loss from the Asian corn borer W chromosome. *BMC Biol* **22:** 102. doi:10.1186/s12915-024-01902-4

Dean R, Mank JE. 2014. The role of sex chromosomes in sexual dimorphism: discordance between molecular and phenotypic data. *J Evolution Biol* **27:** 1443–1453. doi:10.1111/jeb.12345

Dudchenko O, Batra SS, Omer AD, Nyquist SK, Hoeger M, Durand NC, Shamim MS, Machol I, Lander ES, Aiden AP, et al. 2017. De novo assembly of the *Aedes aegypti* genome using Hi-C yields chromosome-length scaffolds. *Science* **356:** 92–95. doi:10.1126/science.aal3327

Dufresnes C, Borzée A, Horn A, Stöck M, Ostini M, Sermier R, Wassef J, Litvinchuck SN, Kosch TA, Waldman B, et al. 2015. Sex-chromosome homomorphy in palearctic tree frogs results from both turnovers and X–Y recombination. *Mol Biol Evol* **32:** 2328–2337. doi:10.1093/molbev/msv113

Dufresnes C, Brelsford A, Baier F, Perrin N. 2021. When sex chromosomes recombine only in the heterogametic sex: heterochiasmy and heterogamety in *Hyla* tree frogs. *Mol Biol Evol* **38:** 192–200. doi:10.1093/molbev/msaa201

Durand NC, Shamim MS, Machol I, Rao SSP, Huntley MH, Lander ES, Aiden EL. 2016. Juicer provides a one-click system for analyzing loop-resolution Hi-C experiments. *Cell Syst* **3:** 95–98. doi:10.1016/j.cels.2016.07.002

Eggert C. 2004. Sex determination: the amphibian models. *Reprod Nutr Dev* **44:** 539–549. doi:10.1051/rnd:2004062

Elinson RP, del Pino EM. 2012. Developmental diversity of amphibians. *WIREs Dev Bio* **1:** 345–369. doi:10.1002/wdev.23

Ellegren H. 2011. Sex-chromosome evolution: recent progress and the influence of male and female heterogamety. *Nat Rev Genet* **12:** 157–166. doi:10.1038/nrg2948

Evans BJ, Alexander Pyron R, Wiens JJ. 2012. Polyploidization and sex chromosome evolution in amphibians. In *Polyploidy and genome evolution* (ed. Soltis PS, Soltis DE), pp. 385–410. Springer, Berlin.

Evans BJ, Mudd AB, Bredeson JV, Furman BLS, Wasonga DV, Lyons JB, Harland RM, Rokhsar DS. 2022. New insights into *Xenopus* sex chromosome genomics from the Marsabit clawed frog *X. borealis*. *J Evol Biol* **35:** 1777–1790. doi:10.1111/jeb.14078

Fahrioglu U, Murphy MW, Zarkower D, Bardwell VJ. 2007. mRNA expression analysis and the molecular basis of neonatal testis defects in Dmrt1 mutant mice. *Sex Dev* **1:** 42–58. doi:10.1159/000096238

Feng Y-J, Blackburn DC, Liang D, Hillis DM, Wake DB, Cannatella DC, Zhang P. 2017. Phylogenomics reveals rapid, simultaneous diversification of three major clades of Gondwanan frogs at the Cretaceous–Paleogene boundary. *Proc Natl Acad Sci* **114:** E5864–E5870. doi:10.1073/pnas.1704632114

Flynn JM, Hubley R, Goubert C, Rosen J, Clark AG, Feschotte C, Smit AF. 2020. Repeatmodeler2 for automated genomic discovery of transposable element families. *Proc Natl Acad Sci* **117:** 9451–9457. doi:10.1073/pnas.1921046117

Furman BLS, Evans BJ. 2018. Divergent evolutionary trajectories of two young, homomorphic, and closely related sex chromosome systems. *Genome Biol Evol* **10:** 742–755. doi:10.1093/gbe/evy045

Furman BLS, Cauret CMS, Knytl M, Song X-Y, Premachandra T, Ofori-Boateng C, Jordan DC, Horb ME, Evans BJ. 2020a. A frog with three sex chromosomes that co-mingle together in nature: *Xenopus tropicalis* has a degenerate W and a Y that evolved from a Z chromosome. *PLoS Genet* **16:** e1009121. doi:10.1371/journal.pgen.1009121

Furman BLS, Metzger DCH, Darolti I, Wright AE, Sandkam BA, Almeida P, Shu JJ, Mank JE. 2020b. Sex chromosome evolution: so many exceptions to the rules. *Genome Biol Evol* **12:** 750–763. doi:10.1093/gbe/evaa081

Goel M, Schneeberger K. 2022. plotsr: visualizing structural similarities and rearrangements between multiple genomes. *Bioinformatics* **38:** 2922–2926. doi:10.1093/bioinformatics/btac196

Goel M, Sun H, Jiao W-B, Schneeberger K. 2019. SyRI: finding genomic rearrangements and local sequence differences from whole-genome assemblies. *Genome Biol* **20:** 277. doi:10.1186/s13059-019-1911-0

Guerrero RF, Kirkpatrick M, Perrin N. 2012. Cryptic recombination in the ever-young sex chromosomes of Hylid frogs. *J Evolution Biol* **25:** 1947–1954. doi:10.1111/j.1420-9101.2012.02591.x

Holt C, Yandell M. 2011. MAKER2: an annotation pipeline and genome-database management tool for second-generation genome projects. *BMC Bioinformatics* **12:** 491. doi:10.1186/1471-2105-12-491

Hudson C, Fu J. 2013. Male-biased sexual size dimorphism, resource defense polygyny, and multiple paternity in the Emei moustache toad (*Leptobrachium boringii*). *PLoS One* **8:** e67502. doi:10.1371/journal.pone.0067502

Iwase M, Satta Y, Hirai Y, Hirai H, Imai H, Takahata N. 2003. The amelogenin loci span an ancient pseudoautosomal boundary in diverse mammalian species. *Proc Natl Acad Sci* **100:** 5258–5263. doi:10.1073/pnas.0635848100

Jeffries DL, Lavanchy G, Sermier R, Sredl MJ, Miura I, Borzée A, Barrow LN, Canestrelli D, Crochet P-A, Dufresnes C, et al. 2018. A rapid rate of sex-chromosome turnover and non-random transitions in true frogs. *Nat Commun* **9:** 4088. doi:10.1038/s41467-018-06517-2

Kabir A, Ieda R, Hosoya S, Fujikawa D, Atsumi K, Tajima S, Nozawa A, Koyama T, Hirase S, Nakamura O, et al. 2022. Repeated translocation of a supergene underlying rapid sex chromosome turnover in *Takifugu* pufferfish. *Proc Natl Acad Sci* **119:** e2121469119. doi:10.1073/pnas.2121469119

Kang HM, Sul JH, Service SK, Zaitlen NA, Kong S-Y, Freimer NB, Sabatti C, Eskin E. 2010. Variance component model to account for sample structure in genome-wide association studies. *Nat Genet* **42:** 348–354. doi:10.1038/ng.548

Kim D, Langmead B, Salzberg SL. 2015. HISAT: a fast spliced aligner with low memory requirements. *Nat Methods* **12:** 357–360. doi:10.1038/nmeth.3317

Koboldt DC, Zhang Q, Larson DE, Shen D, McLellan MD, Lin L, Miller CA, Mardis ER, Ding L, Wilson RK. 2012. VarScan 2: somatic mutation and copy number alteration discovery in cancer by exome sequencing. *Genome Res* **22:** 568–576. doi:10.1101/gr.129684.111

Kondo M, Nagao E, Mitani H, Shima A. 2001. Differences in recombination frequencies during female and male meioses of the sex chromosomes of the medaka, *Oryzias latipes*. *Genet Res* **78:** 23–30. doi:10.1017/S0016672301005109

Koren S, Walenz BP, Berlin K, Miller JR, Bergman NH, Phillippy AM. 2017. Canu: scalable and accurate long-read assembly via adaptive *k*-mer weighting and repeat separation. *Genome Res* **27:** 722–736. doi:10.1101/gr.215087.116

Kosch TA, Crawford AJ, Lockridge Mueller R, Wollenberg Valero KC, Power ML, Rodríguez A, O'Connell LA, Young ND, Skerratt LF. 2025. Comparative analysis of amphibian genomes: an emerging resource for basic and applied research. *Mol Ecol Resour* **25:** e14025. doi:10.1111/1755-0998.14025

Lambert MR, Skelly DK, Ezaz T. 2016. Sex-linked markers in the North American green frog (*Rana clamitans*) developed using DArTseq provide early insight into sex chromosome evolution. *BMC Genomics* **17:** 844. doi:10.1186/s12864-016-3209-x

Langfelder P, Horvath S. 2007. Eigengene networks for studying the relationships between co-expression modules. *BMC Syst Biol* **1:** 54. doi:10.1186/1752-0509-1-54

Ledig S, Röpke A, Wieacker P. 2010. Copy number variants in premature ovarian failure and ovarian dysgenesis. *Sex Dev* **4:** 225–232. doi:10.1159/000314958

Li H. 2018. Minimap2: pairwise alignment for nucleotide sequences. *Bioinformatics* **34:** 3094–3100. doi:10.1093/bioinformatics/bty191

Li H, Durbin R. 2009. Fast and accurate short read alignment with Burrows–Wheeler transform. *Bioinformatics* **25:** 1754–1760. doi:10.1093/bioinformatics/btp324

Li S, Fei L. 1990. A study of the karyotype, C-banding and Ag-NORs on two *Vibrissaphora* toad species (*Pelobatidae Anura*). *J Genet Genom* **17:** 211–215.

Li H, Handsaker B, Wysoker A, Fennell T, Ruan J, Homer N, Marth G, Abecasis G, Durbin R, 1000 Genome Project Data Processing Subgroup. 2009. The Sequence Alignment/Map format and SAMtools. *Bioinformatics* **25:** 2078–2079. doi:10.1093/bioinformatics/btp352

Li C-J, Lin L-T, Tsai H-W, Wen Z-H, Tsui K-H. 2022. Phosphoglycerate mutase family member 5 maintains oocyte quality via mitochondrial dynamic rearrangement during aging. *Aging Cell* **21:** e13546. doi:10.1111/acel.13546

Li J, Fu C, Ai Q, Xie S, Huang C, Zhao M, Fu J, Wu H. 2023. Whole-genome resequencing reveals complex effects of geographical–palaeoclimatic interactions on diversification of moustache toads in East Asia. *Mol Ecol* **32:** 644–659. doi:10.1111/mec.16781

Livernois AM, Graves JAM, Waters PD. 2012. The origin and evolution of vertebrate sex chromosomes and dosage compensation. *Heredity (Edinb)* **108:** 50–58. doi:10.1038/hdy.2011.106

Love MI, Huber W, Anders S. 2014. Moderated estimation of fold change and dispersion for RNA-seq data with DESeq2. *Genome Biol* **15:** 550. doi:10.1186/s13059-014-0550-8

Lynn A, Schrump S, Cherry J, Hassold T, Hunt P. 2005. Sex, not genotype, determines recombination levels in mice. *Am J Hum Genet* **77:** 670–675. doi:10.1086/491718

Ma W-J, Veltsos P. 2021. The diversity and evolution of sex chromosomes in frogs. *Genes (Basel)* **12:** 483. doi:10.3390/genes12040483

Malki S, Nef S, Notarnicola C, Thevenet L, Gasca S, Méjean C, Berta P, Poulat F, Boizet-Bonhoure B. 2005. Prostaglandin D2 induces nuclear import of the sex-determining factor SOX9 via its cAMP-PKA phosphorylation. *EMBO J* **24:** 1798–1809. doi:10.1038/sj.emboj.7600660

Majoros WH, Pertea M, Salzberg SL. 2004. TigrScan and GlimmerHMM: two open source *ab initio* eukaryotic gene-finders. *Bioinformatics* **20:** 2878–2879. doi:10.1093/bioinformatics/bth315

Mank JE. 2009. Sex chromosomes and the evolution of sexual dimorphism: lessons from the genome. *Am Nat* **173:** 141–150. doi:10.1086/595754

Mank JE. 2013. Sex chromosome dosage compensation: definitely not for everyone. *Trends Genet* **29:** 677–683. doi:10.1016/j.tig.2013.07.005

Matsuba C, Merilä J. 2009. Isolation and characterization of 145 polymorphic microsatellite loci for the common frog (*Rana temporaria*). *Mol Ecol Resour* **9:** 555–562. doi:10.1111/j.1755-0998.2008.02368.x

Matsubara K, Tarui H, Toriba M, Yamada K, Nishida-Umehara C, Agata K, Matsuda Y. 2006. Evidence for different origin of sex chromosomes in snakes, birds, and mammals and step-wise differentiation of snake sex chromosomes. *Proc Natl Acad Sci* **103:** 18190–18195. doi:10.1073/pnas.0605274103

Matsui M, Hamidy A, Murphy RW, Khonsue W, Yambun P, Shimada T, Ahmad N, Belabut DM, Jiang J-P. 2010. Phylogenetic relationships of megophryid frogs of the genus *Leptobrachium* (Amphibia, Anura) as revealed by mtDNA gene sequences. *Mol Phylogenet Evol* **56:** 259–272. doi:10.1016/j.ympev.2010.03.014

Mckenna A, Hanna M, Banks E, Sivachenko A, Cibulskis K, Kernytsky A, Garimella K, Altshuler D, Gabriel S, Daly M, et al. 2010. The genome analysis toolkit: a MapReduce framework for analyzing next-generation DNA sequencing data. *Genome Res* **20:** 1297–1303. doi:10.1101/gr.107524.110

Miura I. 1994. Sex chromosome differentiation in the Japanese brown frog, *Rana japonica*. I. Sex-related heteromorphism of the distribution pattern of constitutive heterochromatin in chromosome no. 4 of the Wakuya population. *Zool Sci* **11:** 797–806.

Miura I. 2017. Sex determination and sex chromosomes in amphibia. *Sex Dev* **11:** 298–306. doi:10.1159/000485270

Montgomery SH, Mank JE. 2016. Inferring regulatory change from gene expression: the confounding effects of tissue scaling. *Mol Ecol* **25:** 5114–5128. doi:10.1111/mec.13824

Montiel EE, Badenhorst D, Lee LS, Literman R, Trifonov V, Valenzuela N. 2016. Cytogenetic insights into the evolution of chromosomes and sex determination reveal striking homology of turtle sex chromosomes to amphibian autosomes. *Cytogenet Genome Res* **148:** 292–304. doi:10.1159/000447478

Morescalchi A, Galgano M. 1973. Meiotic chromosomes and their taxonomic value in amphibia anura. *Caldasia* **11:** 41–50.

Morris J, Darolti I, Bloch N, Wright A, Mank J. 2018. Shared and species-specific patterns of nascent Y chromosome evolution in two guppy species. *Genes (Basel)* **9:** 238. doi:10.3390/genes9050238

Natri HM, Shikano T, Merilä J. 2013. Progressive recombination suppression and differentiation in recently evolved neo-sex chromosomes. *Mol Biol Evol* **30:** 1131–1144. doi:10.1093/molbev/mst035

Nurk S, Walenz BP, Rhie A, Vollger MR, Logsdon GA, Grothe R, Miga KH, Eichler EE, Phillippy AM, Koren S. 2020. HiCanu: accurate assembly of segmental duplications, satellites, and allelic variants from high-fidelity long reads. *Genome Res* **30:** 1291–1305. doi:10.1101/gr.263566.120

Omata S, Katagiri C. 1996. Involvement of carbohydrate moieties of the toad egg vitelline coat in binding with fertilizing sperm. *Dev Growth Differ* **38:** 663–672. doi:10.1046/j.1440-169X.1996.t01-5-00010.x

Pan Q, Kay T, Depincé A, Adolfi M, Schartl M, Guiguen Y, Herpin A. 2021. Evolution of master sex determiners: TGF-β signalling pathways at regulatory crossroads. *Phil Trans R Soc B* **376:** 20200091. doi:10.1098/rstb.2020.0091

Perrin N. 2009. Sex reversal: a fountain of youth for sex chromosomes? *Evolution (N Y)* **63:** 3043–3049. doi:10.1111/j.1558-5646.2009.00837.x

Phimphan S, Aiumsumang S. 2021. Chromosomal characteristics of Taolor's stream frog (*Limnonectes taylori*) (Amphibia, Anura) from Thailand. *The Nucleus* **64:** 129–133. doi:10.1007/s13237-019-00291-2

Pincheira-Donoso D, Harvey LP, Grattarola F, Jara M, Cotter SC, Tregenza T, Hodgson DJ. 2021. The multiple origins of sexual size dimorphism in global amphibians. *Global Ecol Biogeogr* **30:** 443–458. doi:10.1111/geb.13230

Ping J, Xia Y, Ran J, Zeng X. 2022. Heterogeneous evolution of sex chromosomes in the torrent frog genus *Amolops*. *Int J Mol Sci* **23:** 11146. doi:10.3390/ijms231911146

Prevot V, Lomniczi A, Corfas G, Ojeda SR. 2005. erbB-1 and erbB-4 receptors act in concert to facilitate female sexual development and mature

reproductive function. *Endocrinology* **146:** 1465–1472. doi:10.1210/en.2004-1146
Quinn A, Juneja P, Jiggins FM. 2014. Estimates of allele-specific expression in *Drosophila* with a single genome sequence and RNA-seq data. *Bioinformatics* **30:** 2603–2610. doi:10.1093/bioinformatics/btu342
Rahman A, Hallgrímsdóttir I, Eisen M, Pachter L. 2018. Association mapping from sequencing reads using *k*-mers. *eLife* **7:** e32920. doi:10.7554/eLife.32920
Rastas P. 2017. Lep-MAP3: robust linkage mapping even for low-coverage whole genome sequencing data. *Bioinformatics* **33:** 3726–3732. doi:10.1093/bioinformatics/btx494
Reddy P, Liu L, Adhikari D, Jagarlamudi K, Rajareddy S, Shen Y, Du C, Tang W, Hämäläinen T, Peng SL, et al. 2008. Oocyte-specific deletion of *Pten* causes premature activation of the primordial follicle pool. *Science* **319:** 611–613. doi:10.1126/science.1152257
Rice WR. 1984. Sex chromosomes and the evolution of sexual dimorphism: lessons from the genome. *Evolution (N Y)* **38:** 735–742. doi:10.2307/2408385
Robinson MD, McCarthy DJ, Smyth GK. 2010. edgeR: a Bioconductor package for differential expression analysis of digital gene expression data. *Bioinformatics* **26:** 139–140. doi:10.1093/bioinformatics/btp616
Rodrigues N, Betto-colliard C, Jourdan-pineau H, Perrin N. 2013. Within-population polymorphism of sex-determination systems in the common frog (*Rana temporaria*). *J Evolution Biol* **26:** 1569–1577. doi:10.1111/jeb.12163
Rodrigues N, Studer T, Dufresnes C, Perrin N. 2018. Sex-chromosome recombination in common frogs brings water to the fountain-of-youth. *Mol Biol Evol* **35:** 942–948. doi:10.1093/molbev/msy008
Ross MT, Grafham DV, Coffey AJ, Scherer S, McLay K, Muzny D, Platzer M, Howell GR, Burrows C, Bird CP, et al. 2005. The DNA sequence of the human X chromosome. *Nature* **434:** 325–337. doi:10.1038/nature03440
Rutkowska J, Badyaev AV. 2008. Meiotic drive and sex determination: molecular and cytological mechanisms of sex ratio adjustment in birds. *Phil Trans R Soc B* **363:** 1675–1686. doi:10.1098/rstb.2007.0006
Sardell JM, Kirkpatrick M. 2020. Sex differences in the recombination landscape. *Am Nat* **195:** 361–379. doi:10.1086/704943
Schartl M, Schmid M, Nanda I. 2016. Dynamics of vertebrate sex chromosome evolution: from equal size to giants and dwarfs. *Chromosoma* **125:** 553–571. doi:10.1007/s00412-015-0569-y
Schmid M, Steinlein C, Bogart JP, Feichtinger W, Haaf T, Nanda I, del Pino EM, Duellman WE, Hedges SB. 2012. The hemiphractid frogs: phylogeny, embryology, life history, and cytogenetics. *Cytogenet Genome Res* **138:** 69–384. doi:10.1159/000343460
Schroeder AL, Metzger KJ, Miller A, Rhen T. 2016. A novel candidate gene for temperature-dependent sex determination in the common snapping turtle. *Genetics* **203:** 557–571. doi:10.1534/genetics.115.182840
Shima JE, McLean DJ, McCarrey JR, Griswold MD. 2004. The murine testicular transcriptome: characterizing gene expression in the testis during the progression of spermatogenesis. *Biol Reprod* **71:** 319–330. doi:10.1095/biolreprod.103.026880
Siberchicot A, Bessy A, Guéguen L, Marais GA. 2017. MareyMap Online: a user-friendly web application and database service for estimating recombination rates using physical and genetic maps. *Genome Biol Evol* **9:** 2506–2509. doi:10.1093/gbe/evx178
Simão FA, Waterhouse RM, Ioannidis P, Kriventseva EV, Zdobnov EM. 2015. BUSCO: assessing genome assembly and annotation completeness with single-copy orthologs. *Bioinformatics* **31:** 3210–3212. doi:10.1093/bioinformatics/btv351
Song X-Y, Furman BLS, Premachandra T, Knytl M, Cauret CMS, Wasonga DV, Measey J, Dworkin I, Evans BJ. 2021. Sex chromosome degeneration, turnover, and sex-biased expression of sex-linked transcripts in African clawed frogs (*Xenopus*). *Phil Trans R Soc B* **376:** 20200095. doi:10.1098/rstb.2020.0095
Stanke M, Keller O, Gunduz I, Hayes A, Waack S, Morgenstern B. 2006. AUGUSTUS: ab initio prediction of alternative transcripts. *Nucleic Acids Res* **34:** W435–W439. doi:10.1093/nar/gkl200
Stevenson KR, Coolon JD, Wittkopp PJ. 2013. Sources of bias in measures of allele-specific expression derived from RNA-seq data aligned to a single reference genome. *BMC Genomics* **14:** 536. doi:10.1186/1471-2164-14-536
Stöck M, Horn A, Grossen C, Lindtke D, Sermier R, Betto-Colliard C, Dufresnes C, Bonjour E, Dumas Z, Luquet E, et al. 2011. Ever-young sex chromosomes in European tree frogs. *PLoS Biol* **9:** e1001062. doi:10.1371/journal.pbio.1001062
Stöck M, Savary R, Betto-Colliard C, Biollay S, Jourdan-Pineau H, Perrin N. 2013. Low rates of X-Y recombination, not turnovers, account for homomorphic sex chromosomes in several diploid species of Palearctic green toads (*Bufo viridis* subgroup). *J Evolution Biol* **26:** 674–682. doi:10.1111/jeb.12086
Tai H-H, Ensor CM, Tong M, Zhou H, Yan F. 2002. Prostaglandin catabolizing enzymes. *Prostag Oth Lipid M* **68–69:** 483–493. doi:10.1016/s0090-6980(02)00050-3
Torres MF, Mathew LS, Ahmed I, Al-Azwani IK, Krueger R, Rivera-Nuñez D, Mohamoud YA, Clark AG, Suhre K, Malek JA. 2018. Genus-wide sequencing supports a two-locus model for sex-determination in Phoenix. *Nat Commun* **9:** 3969. doi:10.1038/s41467-018-06375-y
Veitia R, Nunes M, Brauner R, Doco-Fenzy M, Joanny-Flinois O, Jaubert F, Lortat-Jacob S, Fellous M, McElreavey K. 1997. Deletions of distal 9p associated with 46,XY male to female sex reversal: definition of the breakpoints at 9p23.3–p24.1. *Genomics* **41:** 271–274. doi:10.1006/geno.1997.4648
Vicoso B, Emerson JJ, Zektser Y, Mahajan S, Bachtrog D. 2013. Comparative sex chromosome genomics in snakes: differentiation, evolutionary strata, and lack of global dosage compensation. *PLoS Biol* **11:** e1001643. doi:10.1371/journal.pbio.1001643
Vo LH, Hedrick JL. 2000. Independent and hetero-oligomeric-dependent sperm binding to egg envelope glycoprotein ZPC in *Xenopus laevis*. *Biol Reprod* **62:** 766–774. doi:10.1095/biolreprod62.3.766
Wright AE, Dean R, Zimmer F, Mank JE. 2016. How to make a sex chromosome. *Nat Commun* **7:** 12087. doi:10.1038/ncomms12087
Wu X-N, Wang M-Z, Zhang N, Zhang W, Dong J, Ke M-Y, Xiang J-X, Ma F, Xue F, Hou J-J, et al. 2024. Sex-determining region Y gene promotes liver fibrosis and accounts for sexual dimorphism in its pathophysiology. *J Hepatol* **80:** 928–940. doi:10.1016/j.jhep.2024.01.036
Zhang W, Guo Y, Li J, Huang L, Kazitsa EG, Wu H. 2016. Transcriptome analysis reveals the genetic basis underlying the seasonal development of keratinized nuptial spines in *Leptobrachium boringii*. *BMC Genomics* **17:** 978. doi:10.1186/s12864-016-3295-9
Zheng Y, Li S, Fu J. 2008. A phylogenetic analysis of the frog genera *Vibrissaphora* and *Leptobrachium*, and the correlated evolution of nuptial spine and reversed sexual size dimorphism. *Mol Phylogenet Evol* **46:** 695–707. doi:10.1016/j.ympev.2007.09.019
Zhou Q, Zhang J, Bachtrog D, An N, Huang Q, Jarvis ED, Gilbert MTP, Zhang G. 2014. Complex evolutionary trajectories of sex chromosomes across bird taxa. *Science* **346:** 1246338. doi:10.1126/science.1246338
Zimmer F, Harrison PW, Dessimoz C, Mank JE. 2016. Compensation of dosage-sensitive genes on the chicken Z chromosome. *Genome Biol Evol* **8:** 1233–1242. doi:10.1093/gbe/evw075

Received October 27, 2024; accepted in revised form April 10, 2025.